NONUNIFORM SEDIMENT TRANSPORT MODELING AT GRAYS HARBOR, WA*

ALEJANDRO SANCHEZ[1], WEIMING WU[2]

1. *U.S. Army Engineer Research and Development Center, Coastal and Hydraulics Laboratory, 3909 Halls Ferry Road, Vicksburg, MS 39180-6199, USA. Alejandro.Sanchez@usace.army.mil; Julie.D.Rosati@usace.army.mil.*
2. *National Center for Computational Hydroscience and Engineering, The University of Mississippi, University, MS 38677, USA. wuwm@ncche.olemiss.edu.*

Abstract: A depth-averaged two-dimensional nonuniform sediment transport model is applied to the beaches adjacent to Grays Harbor, WA, USA to test the model skill in predicting nearshore morphology change. The model considers bed material hiding, exposure, sorting, stratification, bed-slope effects, avalanching, non-erodible bed surfaces, and transport due to asymmetrical waves, Stokes drift, roller and undertow. The sediment transport, bed change and sorting equations are solved simultaneously and implicitly at the same time step as the hydrodynamics. The model is able to capture the onshore migration of the offshore bar and filling of the trough but has difficulty in the foreshore region where swash zone processes are neglected. The calculated nearshore water depths agree with measurements with an average Brier Skill Scores of 0.3 and bed changes with an average correlation coefficient R^2 of 0.53.

Introduction

The grain size distribution of coastal sediments is a direct consequence of the sediment sources and hydrodynamic conditions that exist in each specific environment. Mason and Folk (1958) showed that sediments in different coastal environments can be distinguished by their statistical parameters such as mean, standard deviation (sorting) and skewness. For most beaches, coarser sediment is generally found in the swash zone and the wave breaker line while finer sediment is found in the trough, landward of the breaker line (e.g. Mason and Folk, 1958; Ping et al., 1998). As reported in Mason and Folk (1958), in most beaches the sediments are negatively skewed (coarser grained) because the fine sediments are winnowed away by breaking waves. In general, finer sediments are found in areas of flow deceleration and vice-versa (e.g. Black et al., 1989). Many coastal inlets have shell-lag deposits in the inlet throat which armors the and prevents excessive erosion. Bed material textural changes can also be related to storm events, seasonal climatic changes and long-term depositional and erosional trends due to changes in the amount or properties of the sediment source(s). For example, Ping et al. (1998)

* All figures are in color on the Coastal Sediments Proceedings DVD.

found that storms and the resulting offshore migration of the bar could leave a layer of coarser lag deposit where fine deposits would normally be found.

The Coastal Modeling System (CMS) developed by the U.S. Army Corps of Engineers (Buttolph et al., 2006; Lin et al., 2008) is an integrated wave, hydrodynamic, sediment transport and morphology change modeling system. The CMS has previously been validated at Grays Harbor for hydrodynamics and waves in Lin et al. (2008) and Wu et al. (2010, 2011). In this paper, a depth-averaged two-dimensional (2DH) nonuniform total load sediment transport model is added to the CMS and applied to Grays Harbor, WA, USA in order to test the model performance in predicting nearshore morphology change and distribution of nearshore sediments. The model uses a multi-fraction method in which the sediment mixture is divided into discrete fractions and the total sediment transport rate is obtained as the sum of the individual fractional transport rates. The bed is also divided into discrete layers and the fractional composition of each sediment layer is simulated in time. The model also includes transport over nonerodible bed surfaces, avalanching, and cross-shore transport due to wave asymmetry, roller, and undertow.

Nonuniform Sediment Transport Model

The single-sized sediment transport model described in Sánchez and Wu (2011) is extended to multiple-sized nonuniform sediments. In this model, the sediment transport is separated into current- and wave-related transports. The transport due to currents includes the stirring effect of waves; and the wave-related transport includes the transport due to asymmetric oscillatory wave motion and also steady contributions by Stokes drift, surface roller, and undertow. The current-related bed and suspended transports are combined into a single total-load transport equation, thus reducing the computational costs and simplifying the bed change computation. The 2DH transport equation for the current-related total load is

$$\frac{\partial}{\partial t}\left(\frac{hC_{tk}}{\beta_{tk}}\right)+\frac{\partial\left(U_j hC_{tk}\right)}{\partial x_j}=\frac{\partial}{\partial x_j}\left[\nu_s h\frac{\partial\left(r_{sk}C_{tk}\right)}{\partial x_j}\right]+\alpha_t\omega_{sk}\left(C_{t*k}-C_{tk}\right) \qquad (1)$$

for $j=1,2;\ k=1,2,...,N$, where N is the number of sediment size classes, t is time, h is the total water depth, x_j is the Cartesian coordinate in the jth direction, U_j is the depth-averaged current velocity, C_{tk} is the depth-averaged total-load sediment concentration, β_{tk} is the total-load correction factor, r_{sk} is the fraction of suspended load in total load (equal to 1 for fine-grained sediments), ν_s is the sediment mixing coefficient, α_t is the total-load adaptation coefficient and ω_{sk} is the sediment fall

velocity. The equilibrium concentration is calculated as $C_{t*k} = p_{bk} C_{tk}^*$ where p_{bk} is fraction of the k^{th} sediment size class in the top-most bed layer and C_{tk}^* is the potential equilibrium sediment concentration calculated from empirical formulas. The hiding and exposure of each bed material size class are considered by modifying the critical shields parameter using the method of Wu et al. (2000).

The correction factor β_{tk} is the ratio of the depth-averaged sediment and flow velocities and accounts for the vertical nonuniform profiles of sediment concentration and current velocity. In a combined bed load and suspended load model, the correction factor is given by $\beta_{tk} = 1/\left[r_{sk} / \beta_{sk} + (1 - r_{sk})U / u_{bk}\right]$ where u_{bk} is the bed load velocity and β_{tk} is the suspended load correction factor and is defined as the ratio of the depth-averaged sediment and flow velocities. Because most of the sediment is transported near the bed, both the total and suspended load correction factors are usually less than 1 and typically in the range of 0.3 and 0.7, respectively. By assuming logarithmic current velocity and exponential suspended sediment concentration profiles, an explicit expression for the suspended load correction factor β_{sk} may be obtained as

$$\beta_s = \frac{\int_a^h ucdz}{U\int_a^h cdz} = \frac{\mathrm{E}_1(\phi A) - \mathrm{E}_1(\phi) + \ln(A/Z)\,\mathrm{e}^{-\phi A} - \ln(1/Z)\,\mathrm{e}^{-\phi}}{\mathrm{e}^{-\phi A}\left[\ln(1/Z) - 1\right]\left[1 - \mathrm{e}^{-\phi(1-A)}\right]} \tag{2}$$

where $\phi = \omega_s h / \varepsilon$, $A = a/h$, $Z = z_0 / h$, ε is the vertical mixing coefficient, and E_1 is the exponential integral. The equation can be further simplified by assuming that the reference height is proportional to the roughness height (e.g. $a = 30 z_0$), so that $\beta_s(Z, \phi)$.

The fractional bed change is calculated as

$$\left(1 - p_m'\right)\left(\frac{\partial \zeta}{\partial t}\right)_k = \alpha_t \omega_{sk}\left(C_{tk*} - C_{tk}\right) - \frac{\partial Q_{wk,j}}{\partial x_j} + \frac{\partial}{\partial x_j}\left(D_s \left|Q_{bk}\right| \frac{\partial \zeta}{\partial x_j}\right) \tag{3}$$

where ζ is the still water depth, p_m' is the bed porosity, Q_{wk} is the sediment transport due to wave asymmetry, Stokes Drift, roller and undertow, D_s is a bed-slope coefficient, and $Q_{bk} = hUC_{tk}(1\text{-}r_{sk})$ is the bed load. The total bed change is calculated as the sum of Eq. (2) for all size classes. The advantage of including Q_{wk} in the bed change equation instead of the transport equation is that it simplifies the

calculation and has been found to improve model stability. In addition, it is not straightforward to include the wave-related transport in Eq. (1), since modifications would need to be made to the total load correction factor and adaptation coefficient. For simplicity, it is assumed that the onshore and offshore components are on the same axis as the waves. Details on Q_{wk} are left for a later publication.

The bed material above the erodible layer is divided into multiple layers, and the sorting of sediments is calculated using the mixing layer concept. The mixing layer is the top-most (first) layer of the bed. The temporal variation of the bed-material composition in each layer is calculated using a method similar to Wu (2004). The sediment transport, bed change, and bed gradation are solved simultaneously (coupled), but are decoupled from the flow calculation at the time step level. To illustrate the bed layering process, Figure 1 shows an example of the temporal evolution of 7 bed layers during erosional and depositional regimes. Details on the mixing layer thickness calculation and the bed layering algorithm are left for a subsequent publication.

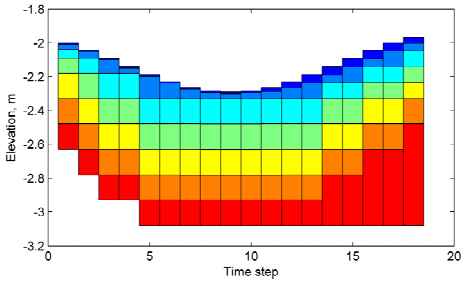

Fig. 1. Schematic showing an example bed layer evolution. Colors indicate layer number.

Field Study

Grays Harbor inlet, WA is located on the southwest Washington coast, USA, at the mouth of the Chehalis River. Between May and July of 2001, the U.S. Geological Survey instrumented 6 tripods and collected time series of wave height, water surface elevation, near-bottom current velocity, and sediment concentration proxies (Landerman et al., 2004). Weekly topographic maps and monthly bathymetric surveys along transects spaced 50-200 m apart were collected (see Figure 2). In addition grab sample of surface sediment were collected at several locations. Figure 1 shows the location of the observation stations and monthly nearshore bathymetric profiles.

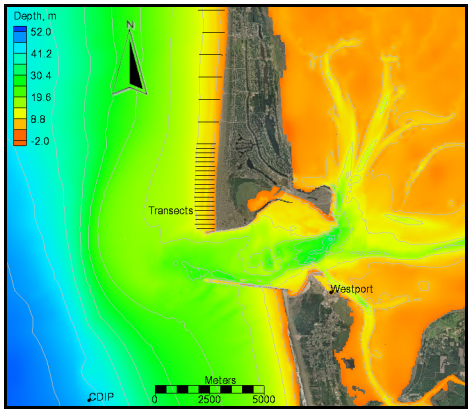

Fig. 2. Map of Grays Harbor inlet, WA showing the location of the nearshore bathymetric transects.

Model Setup

The first half of the field deployment between May 6-30 of 2001 was simulated. The simulation period was characterized by relatively calm conditions, with a few spring storms with significant wave heights on the order of 3 m (see Figure 3).The spectral wave transformation model CMS-Wave was run on a ~200,000 cell Cartesian grid with varying grid resolution from 15-120 m (see Figure 4). The waves were forced with spectral wave information from the Coastal Data Information Program (CDIP) buoy No. 03601 located southwest of the inlet at a depth of 42 m (see Figure 2).

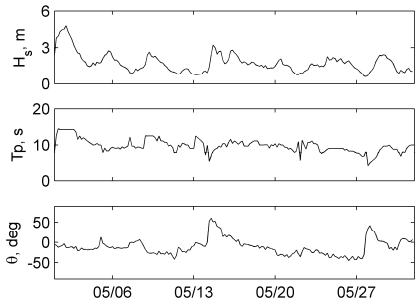

Fig. 3. Time series of significant wave height (top), peak wave period (middle), and incident wave angle with respect to shore line (bottom) during May 2001.

The CMS-Flow was forced with a water level time series from Westport Harbor with a negative 30 min phase lag correction which was obtained by comparing with the stations deployed during the field study (see Figure 5). Winds were interpolated from the Blended Sea Winds product of the National Climatic Data Center (Zhang

et al. 2006). The Manning's coefficient was calibrated in previous studies as 0.018 over the whole domain except on the rock structures where a value of 0.1 was used. A flux boundary condition was applied at the Chehalis River which was obtained from the USGS. The CMS-Flow ~55,000-cell quadtree grid is shown in Figure 6 and has six levels of refinement from 20-640 m. A variable time step was used with a maximum value of 10 min. The sediment transport and bed change were calculated at every hydrodynamic time step.

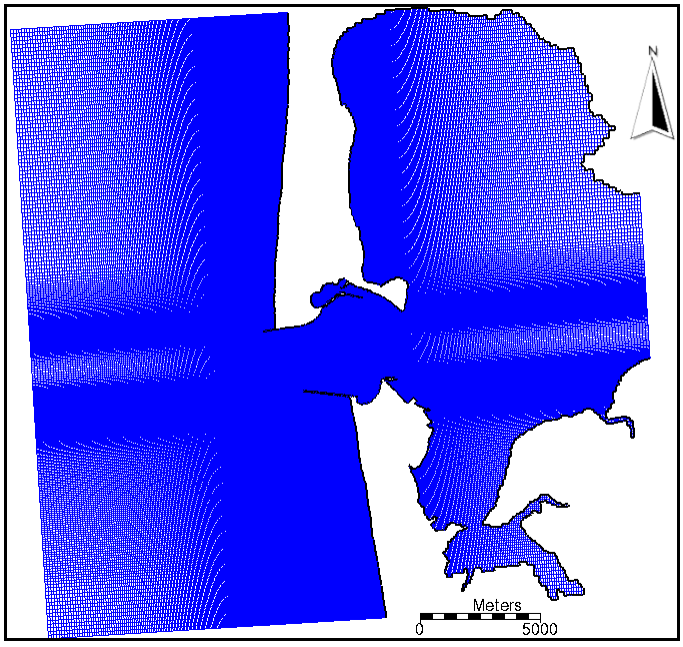

Fig. 4. Nonuniform Cartesian grid used for CMS-Wave.

A ramp or spin up period of 5 days was implemented based on previous hydrodynamic studies at Grays Harbor so the start of the simulation was May 1, 2001. Waves were calculated at a constant 2 hr interval (steering interval). The significant wave height, peak wave period, wave unit vectors, and wave dissipation were linearly interpolated to the flow grid every steering interval and then linearly interpolated in time at every hydrodynamic time step. Wave variables such as wave length and bottom orbital velocities were updated every time step for wave-current interaction. When using such a large steering interval, it is important to consider how the water levels, current velocities and bed elevations, which are passed from the flow to the wave model, are estimated. For this application, and for most open coast applications, the nearshore waves are most sensitive to variations in water levels and not currents. Therefore, improved results can be obtained by predicting

the water levels at the wave model time step based on a decomposition of the water levels into spatially constant and variable components. The spatially constant component is assumed to be equal to the tidal water surface elevation and the spatially variable component which includes wind and wave setup is estimated based on the last flow time step. The currents and bed elevations which are passed from the wave to flow grid are simply set to the last time step value. Other types of prediction methods could be used; however, the approach described above has been found to be sufficient for most applications and is simple to calculate. After each wave run, a surface roller model is also calculated on the wave grid and the roller stresses are added to the wave stresses before interpolating on to the flow grid. Even though CMS-Flow and CMS-Wave use different grids, the two models are in a single code which facilitates the model coupling and speeds up the computation by avoiding communication files, variable allocation and model initialization at every steering interval.

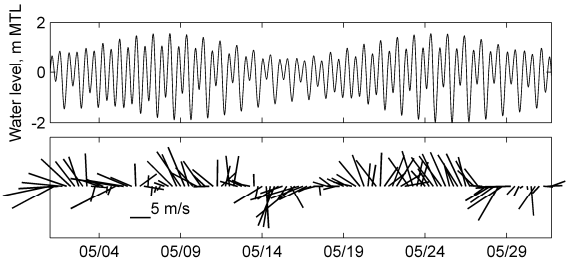

Fig. 5. Water levels (top) and wind velocities and direction (bottom) during May of 2001.

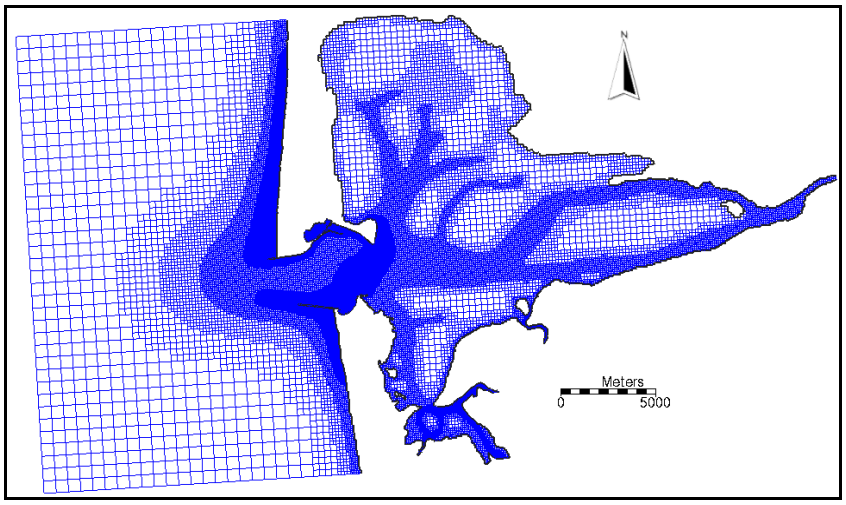

Fig. 6. Quadtree grid used for CMS-Flow.

The initial bed material composition was specified by a spatially variable median grain size d_{50} and constant geometric standard deviation σ_g of 1.3 mm based on field measurements. The initial fractional composition at each cell was assumed to be constant in depth and have a log-normal distribution, and represented by six size classes with characteristic diameters of 0.1, 0.126, 0.16, 0.2, 0.25, and 0.31 mm. An example of the initial grain size distribution is shown in Figure 7. Ten bed layers were used with an initial thickness of 0.5 m each. The Lund-CIRP transport formulas were used to estimate the transport capacity (Camenen and Larson, 2007). The total-load adaptation coefficient is calculated as $\alpha_t = Uh/(L_t\omega_s)$ where L_t is the total-load adaptation length. Here $L_t = (1-r_s)L_b + r_s L_s$, where L_b and L_s are the bed- and suspended-load adaptation lengths, respectively. The bed-load adaptation length is set to 10 m, and the suspended-load adaptation length is calculated as $L_s = Uh/(\alpha_s\omega_s)$ where the suspended-load adaptation coefficient α_s is set to 0.5. A constant bed porosity of 0.3 was used in the simulation. The bed load velocity is calculated using Van Rijn's (1984) formula with recalibrated coefficients by Wu et al. (2006).

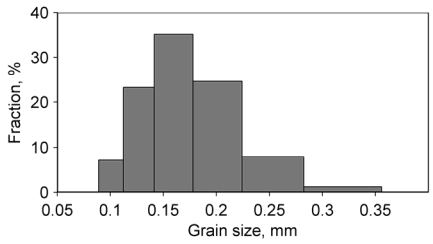

Fig. 7. Example log-normal grain size distribution (d_{50} = 0.16 mm, σ_g = 1.3 mm).

Results and Discussion

Calculations were performed on a desktop PC and the 31 days simulation was completed in approximately 10 hrs. A comparison of the measured and computed bed changes between May 6 and 30 of 2001 is shown in Figure 8. Selected regions of interest are encompassed by black lines in order to help visually compare the bed changes. In general, the results show many common features and similar erosion and deposition patterns. More specifically, the bed change is characterized by the erosion of the outer bar, deposition in the inner bar face and outer trough, and erosion of the inner trough face. There is a region extending approximately 1 km from the northern jetty, where the bed changes are noticeably different from those further to the north. This region is interpreted as being strongly influenced by the presence of the inlet, ebb shoal and northern jetty. As an example, Figure 9 shows a snap shot of the current velocities on May 14, 2001 during an ebb tide and

southeasterly swell in which there is a reverseal in the longshore current in the transition region due to the combined effect of refraction of waves over the ebb shoal, deflection of the ebb current by the northern jetty, and formation of the northern ebb jet gyre. This emphasizes the importance of accurately capturing the inlet dynamics in modeling adjacent beaches. Interestingly, both the measurements and model results show small (200-300 m in length) inner bars form adjacent to the trough, which appear to occur at regular 400-500 m intervals.

The computed bed changes in the foreshore region (beach face) are relatively small compared to the measurements due to the lack of swash zone processes in the present version of CMS. Swash zone processes enhance transport in the surf zone by increasing the current velocities, transport rates and mixing at the shoreline. Large component of longshore sediment transport occurs in the swash zone and without these processes, morphodynamic models will tend to underestimate longshore transport rates and bed change in the foreshore region.. Walstra et al. (2005) simulated the bed change at transects 9 and 20 using a two-dimensional vertical (2DV) profile evolution model and were able to predict the onshore migration of the bar, but also found that the model performance deteriorates in the foreshore region.

The measured and computed water depths and bed changes for Transects 1 and 9 are shown in Figure 10. As observed in Figure 8, most of bed changes occurred from the nearshore bar to the outer beach face. The model was able to accurately predict an onshore bar migration although it underestimated the nearshore bar height which is also observed in Figure 8. In order to evaluate the model performance in predicting the nearshore bathymetry, the Brier Skill Score *BSS* was applied to the water depths and the correlation coefficient R^2 to the bed change. Other goodness of fit parameters were also calculated and showed similar patterns, for simplicity only the previously mentioned parameters are shown in Figure 10. The goodness of fit statistics show a wide range of values.

The measured bed change shows a larger variation as compared to the model results. indicating that morphology change is sensitive to longshore variations in forcing, initial bathymetry or 3D processes such as rip currents. As discussed by Walstra et al. (2005), the model results indicate that the waves and currents do in fact vary over the spatial scales (10-100 m) of the observed morphological variations. As an example, Figure 12 shows a snap shot of the current velocities during an ebb tide and easterly wave event (approximately normal to shore) on May 6, 2001 which shows complex nearshore currents, several reversals in the direction of the longshore current and the influence of the ebb jet gyre.

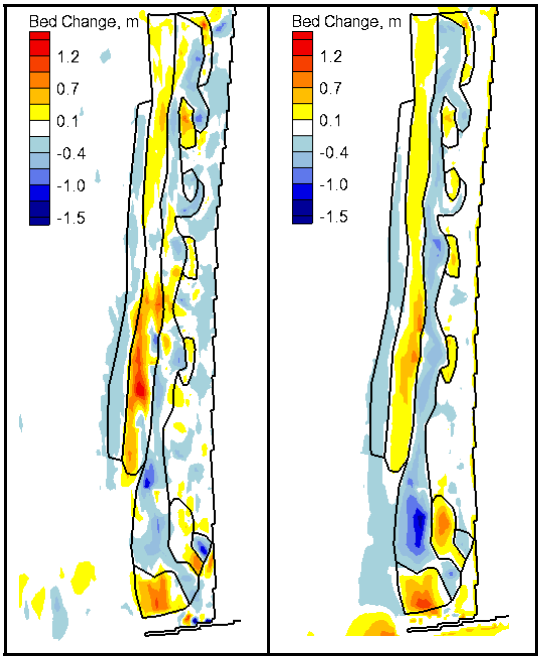

Fig. 8. Measured (left) and computed (right) bed changes between May 6 and 30, 2001.

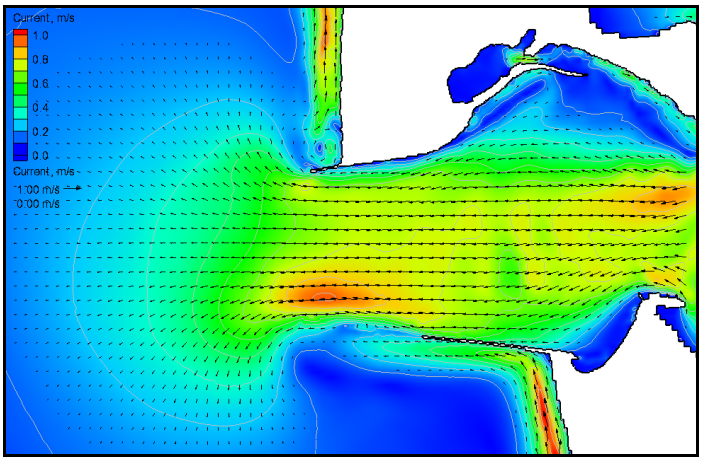

Fig. 9. Snapshot of current magnitudes during an ebb tide on May 14, 2001.

Although the field measurements show evidence of stratification, no measurements were conducted in the surf zone where most of the bed change occurred. It is expected that due to the strong mixing in the surf zone, the 2DH model is a

reasonable approximation. In addition, previous studies at Grays Harbor (Wu et al. 2010, 2011) have found good agreement with hydrodynamic measurements and sediment transport patterns using a 2DH approach.

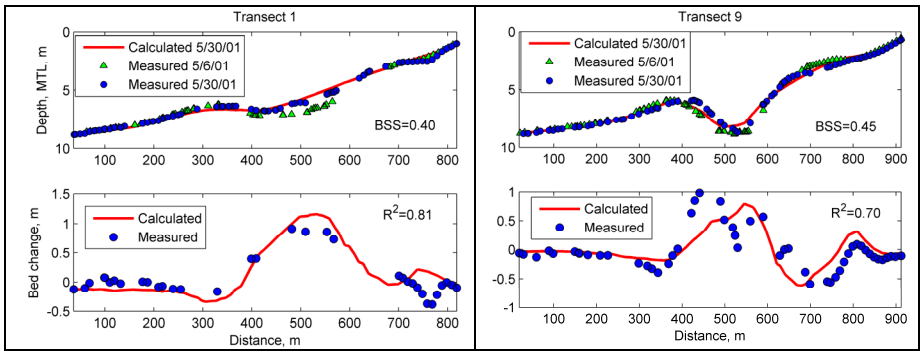

Fig. 10. Measured and computed water depths (top) and bed changes (bottom) for Transect 9.

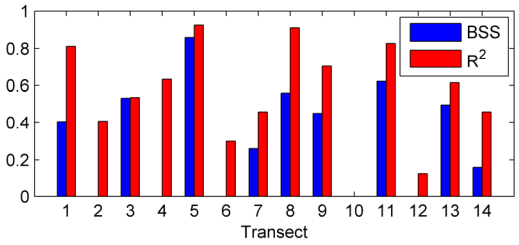

Fig. 11. Brier Skill Score for water depths and correlation coefficient for computed bed changes at selected Transects.

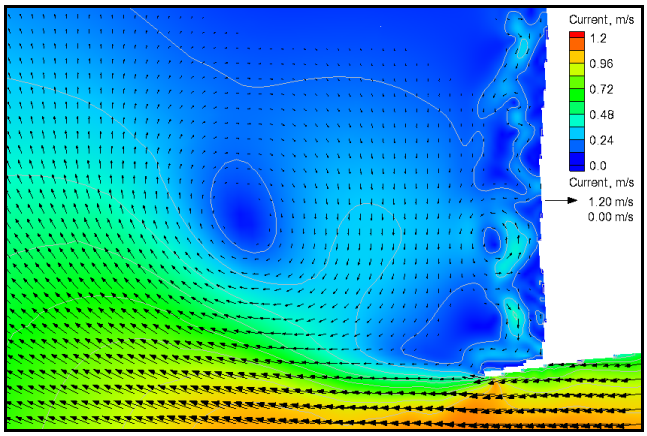

Fig. 12. Snap shot of current magnitudes during an ebb tide on May 6, 2001.

The computed median grain size on May 30, 2001 is shown in Figure 13. Qualitatively, the results agree well with field measurements and typical findings for most inlets and beaches. Coarser sediments are found in the beach face and breaker line (offshore bar) and finer sediments are found in the trough and offshore of the surf zone. In addition, coarser sediments are found in the inlet entrance and finer sediments are found on the periphery of the ebb shoal. In addition, it is noted that the area around the jetties highly armored due to the strong currents and large waves present, which is also observed in field.

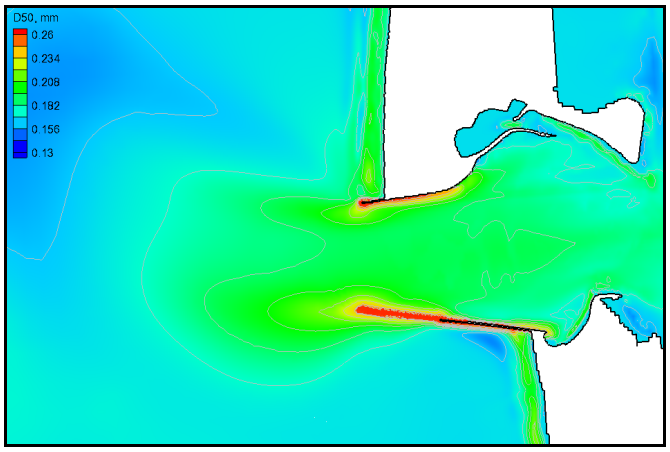

Fig. 13. Distribution of median grain size calculated after the 25-day simulation.

Conclusion

A depth-averaged nonuniform sediment transport model has been developed and applied to Grays Harbor, WA. Nearshore measurements of bathymetry were used to validate the model during the period of May 6-30, 2001. Goodness of fit statistics of water depths and bed changes, indicate generally reasonable to good model performance although the model skill varied significantly, especially on the beach face where swash zone processes are likely important and are not presently represented in the model. The measured bed change shows larger degree of variability as compared to model results indicating that nearshore morphology is sensitive to longshore variations in forcing and cross-shore processes which are difficult to resolve. Results also show that there is a region adjacent to the north jetty (transition zone) which is strongly influenced by the presence of the inlet due to wave refraction over the ebb-tidal delta, ebb and flood currents including detached eddies, and the presence of the north jetty.

Acknowledgments

This work was conducted in part through funding from the ‘‘Coastal Modeling System’’ work unit of the Coastal Inlets Research Program of the U.S. Army Corps of Engineers. Permission was granted by the Chief, U. S. Army Corps of Engineers to publish this information. We appreciate Dr. Julie D. Rosati for reviewing the manuscript the help and support of Dr. Lihwa Lin, Dr. Honghai Li, Mr. Mitch Brown, and Dr. Alan Zundel.

References

Black, K. P., Healy, T. R., and Hunter, M. G. (1989). “Sediment dynamics in the lower section of a mixed sand shell-lagged tidal estuary, New Zealand”, Journal of Coastal Research, 5(3), 503-521.

Buttolph, A. M., Reed, C. W., Kraus, N. C., Ono, N., Larson, M., Camenen, B., Hanson, H.,Wamsley, T., and Zundel, A. K. (2006). “Two-dimensional depth-averaged circulation model CMS-M2D: Version 3.0, Report 2: Sediment transport and morphology change,” *Tech. Rep. ERDC/CHL TR-06-9*, U.S. Army Engineer Research and Development Center, Coastal and Hydraulic Engineering, Vicksburg, MS.

Camenen, B., and Larson, M. (2007). “A unified sediment transport formulation for coastal inlet applications,” *Tech. Rep. ERDC/CHL TR-07-1*, U.S. Army Engineer Research and Development Center, Coastal and Hydraulic Engineering, Vicksburg, MS.

Landerman, L., Sherwood, C. R., Gelfenbaum, G., Lacy, J., Ruggiero, P., Wilson, D., Chrisholm, T., and Kurrus, K. (2004). “Grays Harbor Sediment Transport Experiment: Spring 2001 – Data Report,” U.S. Geological Survey Data Series.

Lin, L., Demirbilek, Z., Mase, H., Zheng, J., Yamada, F. (2008). “CMS-wave: a nearshore spectral wave processes model for coastal inlets and navigation projects.” *Tech. Rep. ERDC/CHL-TR-08-13*, U.S. Army Engineer Research and Development Center, Coastal and Hydraulics Laboratory, Vicksburg, MS.

Mason, C. C., and Folk. R. L. (1958). “Differentiation of beach, dune and eolian flat environments by size analysis: Mustang Island, Texas,” *Journal of Sedimentary Petrology*, 28(2), 211-226.

Ping, W., Davis, R. A., and Kraus, N. C. (1998). "Cross-shore distribution of sediment texture under breaking waves along low-wave-energy coasts," *Journal of Sedimentary Research*, 68(3), 497-506.

Sánchez, A., and Wu, W. (2011). "A non-equilibrium sediment transport model for coastal inlets and navigation channels," *Journal of Coastal Research*, [In Press]

Van Rijn, L.C. (1984). "Sediment transport, part I: bed load transport," *Journal of Hydraulic Engineering*, ASCE, 110(10), 1431-1456.

Walstra, D.R, Ruggiero, P., Lesser, G., and Gelfenbaum, G. (2005). "Modeling nearshore morphological evolution at seasonal scale," Proceedings of the 5th International Conference on Coastal Dynamics, Barcelona, Spain.

Wu, W. (2004). "Depth-averaged 2-D numerical modeling of unsteady flow and nonuniform sediment transport in open channels," *Journal of Hydraulic Engineering*, ASCE, 135(10) 1013-1024.

Wu, W., Altinakar, M., and Wang, S.S.Y. (2006). "Depth-averaged analysis of hysterersis between flow and sediment transport under unsteady conditions," *International Journal of Sediment Research*, 21(2), 101-112.

Wu, W., Sánchez, A., and Mingliang, Z. (2011). "An implicit 2-D shallow water flow model on an unstructured quadtree rectangular grid," *Journal of Coastal Research*, [In Press]

Wu, W., Sánchez, A., and Mingliang, Z. (2010). "An implicit 2-D depth-averaged finite-volume model of flow and sediment transport in coastal waters," *Proceeding of the International Conference on Coastal Engineering*, [In Press]

Wu, W., Wang, S.S.Y., and Jia, Y. (2000). "Nonuniform sediment transport in alluvial rivers," Journal of Hydraulic Research, IAHR, 38(6), 427-434.

Zhang, H.-M., Reynolds, R. W., and Bates, J. J. (2006). "Blended and Gridded High Resolution Global Sea Surface Wind Speed and Climatology from Multiple Satellites: 1987 – Present" *American Meteorological Society 2006 Annual Meeting*, Paper #P2.23, Atlanta, GA, January 29 - February 2, 2006.